Flow dynamics in Models of Intracranial Terminal Aneurysms

Alvaro Valencia[1]

Abstract: Flow dynamics play an important role in the pathogenesis and treatment of intracranial aneurysms. The evaluation of the velocity field in the aneurysm dome and neck is important for the correct placement of endovascular coils, and the temporal and spatial variations of wall shear stress in the aneurysm are correlated with its growth and rupture. This numerical investigation describes the hemodynamic in two models of terminal aneurysm of the basilar artery. Aneurysm models with a aspect ratio of 1.0 and 1.67 were studied. Each model was subject to physiological representative waveform of inflow for a mean Reynolds number of 560. The effects of symmetric and asymmetric outflow conditions in the branches were studied.

The three dimensional continuity and Navier-Stokes equations for incompressible, unsteady laminar flow with Newtonian properties were solved with a commercial software using non structured fine grids with 197807 and 202515 tetrahedral cells for the model 1 and 2 respectively.

The flow shows complex vortex structure in both models, the inflow and outflow zones in the aneurysm neck were determined. The wall shear stress on the aneurysm showed big temporal and spatial variations. The asymmetric outflow increased the wall shear stress on the aneurysm only in model 1.

keyword: aneurysm, basilar artery, CFD, unsteady flow, wall shear stress.

1 Introduction

The flow in arteries is dominated by unsteady phenomena. The Womersley number characterizes the unsteady flow in the different arteries. In certain circumstances,

[1] Department of Mechanical Engineering
Universidad de Chile
Casilla 2777, Santiago, Chile
e-mail: alvalenc@ing.uchile.cl,
Tel.:+56-2-6784386, Fax:+56-2-6988453

unusual hemodynamic conditions create an abnormal biological response, Ku (1997). The relationship between flow in the arteries, particularly the wall shear stress, and the sites where diseases develop have motivated much of the research on arterial flow in recent decades. It is now well accepted that in sites where shear stresses are low, or change rapidly in time or space are most vulnerable. These conditions are likely to prevail at places where the vessel is curved or bifurcates, Berger and Jou (2000).

When an arterial wall loses its structural integrity, the result is growth of a balloon-like bulge called a saccular aneurysm. The cerebral saccular aneurysm is a pathological dilation of an artery, generally found in and about the circle of Willis. Saccular aneurysms initiating at arterial bifurcations or along the cavernous segments of intracranial arteries may be of the lateral or terminal type. Saccular aneurysms display a variety of sizes and complex shapes, Parlea et al. (1999).The majority of intracranial aneurysms are located in the anterior circulation, most commonly at the junction of the internal carotid artery and the posterior communicating artery complex. Aneurysms of the posterior circulation are most frequently located at the bifurcation of the basilar artery or the junction of a vertebral artery and the ipsilateral posterior inferior cerebellar artery, Schievink (1997). Rupture of an intracranial saccular aneurysm generally causes subarachnoid hemorrhage with severe neurological complications.

Hemodynamic factors, such a blood velocity, change in wall shear stress and pressure, play important roles in the pathogenesis of aneurysms and thrombosis. Fluid flow in an aneurysm generally depends upon its geometric configuration and relation to the parent vessel, the size of the orifice and the volume of the aneurysm, Weir et al. (2003). The classical treatments of saccular aneurysms are direct surgical clipping or endovascular coil insertion. However certain intracranial aneurysms, because of their fusiform or complex wide-necked structure, giant size, or involvement with critical perforating or branch vessels, are unamenable with these treatments. Actually

proximal and distal occlusion (trapping) is the most effective treatment of these lesions. In lesions that cannot be trapped, alteration in blood flow to the inflow zone, the site most vulnerable to aneurysm growth and rupture, is used, Hoh et al. (2001). This strategy is based on the premise that aneurysm growth and rupture are functions of shear stress at the inflow zone. If the flow into the aneurysm can be altered such the shear stress at the inflow zone can be reduced, it may be possible that the history of the lesion can be altered. For these reasons hemodynamic studies on models of saccular aneurysms are very important to obtain quantitative criteria for their treatments.

Liou and Liou (1999) presented a review of in vitro studies of hemodynamic characteristics in terminal and lateral aneurysm models. They reported in terminal aneurysms that with uneven branch flow, the flow activity inside the aneurysm and the shear stresses acting on the intra aneurismal wall increase with increasing bifurcation angle. There also exists a middle range of aneurysm size, above and below which the forced vortex inside a terminal aneurysm is weaker, whereas in the middle range of aneurismal size, the forced vortex is stronger, and the fluctuation level is higher near the dome. In other words, the dome of a mid size terminal aneurysm is subject to larger wall shear stress and vibrations. Ernemann et al (2003) reported the influence of geometrical parameters on hemodynamic in vitro models of aneurysms obtained with three dimensional rotational angiography. Tateshima et al. (2001, 2003) studied the intra aneurismal flow dynamics in acrylic models obtained using three dimensional computerized tomography angiography, they showed that the axial flow velocity structures were dynamically altered throughout the cardiac cycle, particularly at the aneurysm neck. The endovascular treatment of aneurysms may benefit from an accurate determination of flow patterns in the aneurysm neck and dome. Although aneurysm rupture is thought to be associated with a significant change in aneurysm size, there is still great controversy regarding the size at which rupture occurs. Rupture occurs preferentially at the site of dome, particularly in daughter aneurysms. The relationship between geometric features and rupture is closely associated with very low flow conditions, Ujiie et al. (1999).

Foutrakis et al. (1999) have presented two dimensional simulation of fluid flow in curved arteries and arterial bifurcations and the relationship of these hemodynamics to aneurysm formation and growth. The results suggest that the shear stress that develops along the outer wall of a curved artery and at the apex of an arterial bifurcation create a hemodynamic state that promotes saccular aneurysm formation. Recently Steinman et al. (2003) reported image-based computational simulation of the flow dynamics for Newtonian fluid in a giant anatomically realistic human intracranial aneurysm with rigid walls. The analysis revealed high-speed flow entering the aneurysm at the proximal and distal ends of the neck, promoting the formation of both persistent and transient vortices within the aneurysm sac. This produced dynamic patterns of elevated and oscillatory wall shear stresses distal to the neck and along the sidewalls of the aneurysm.

The influence of the non-Newtonian properties of blood on the flow in arteries was investigated by Gijsen et al. (1999). They performed laser Doppler anemometry experiments and finite element simulations of steady flow in a three dimensional model of the carotid bifurcation. A comparison between the experimental and numerical results showed good agreement, both for the Newtonian and the non-Newtonian fluid. Zhao et al. (2000) have studied the flow in a model of a human carotid arterial bifurcation with rigid and compliant wall assumptions. Generally there is a reduction in the magnitude of wall shear stress with compliant wall, with its degree depending on location and phase of the cardiac motion. The local differences are however not big, and the influence of compliant arterial wall can be considered as second order effect compared to the influence of geometry and flow pulsatility.

Recently Cole et al. (2004) performed flow visualization and particle imaging velocimetry on models of bifurcation saccular aneurysm in the basilar artery. Two flow models of varying spherical dome size were constructed out of clear silicone. Each model was subject to steady input flow conditions for a range of Re=175-650. They performed also experiments with pulsatile input flow conditions at a mean Re=560 with both sinusoidal and physiologically representative waveform. Physiological and sinusoidal pulsatile input conditions with an asymmetric branching ratio caused a periodic appearance of a vortex-like circulation pattern in the dome of the smaller model. Planar instantaneous velocity field measurements showed highly three dimensional flow patterns for the unsteady cases. The time dependence of
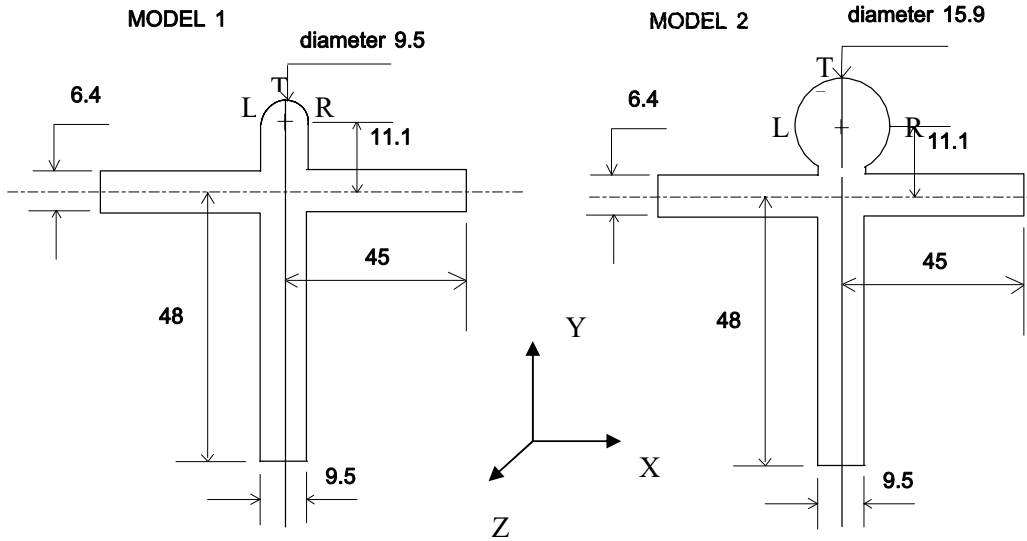
Figure 1 : Flow model geometries.

wall shear stress showed high amplitude with pulsatile inflow.

This paper presents detailed numerical simulations of unsteady flow in two models of terminal saccular aneurysm of the basilar artery, the geometry was taken similar to the experimental work of Cole et al. (2004). The effects of aneurysm geometry and branches flow-rate ratio on flow characteristics and shear stress on the aneurismal wall are reported and discussed in this work.

2 Mathematical Model and Geometry

The fluid flow in the basilar artery is described by the continuity and Navier-Stokes equations for a Newtonian fluid:

$$\vec{\nabla} \cdot \vec{u} = 0 \tag{1}$$

$$\rho \frac{\partial \vec{u}}{\partial t} + \rho (\vec{u} \cdot \vec{\nabla}) \vec{u} = -\vec{\nabla} p + \mu \nabla^2 \vec{u} \tag{2}$$

In this work, the effects of non-Newtonian fluid properties, wall elasticity, and anatomically realistic model are no considered, as discussed in the introduction. The geometry of the two models of terminal aneurysm in the basilar artery is shown in Fig. 1. The bifurcation angle is 90°, with symmetric placement of outflow tubes. Along with an aneurysm dome located symmetrically at the end of the input tube, the models form an idealized "T" shape. Physiologically, bifurcation geometry and aneurysm location exhibit a great amount of irregularity

and asymmetry. This work mimics the flow conditions created by geometrical asymmetry by causing an asymmetric branching ratio of flow between the outflow tubes. Therefore cases with symmetric and asymmetric outflow were studied, for the cases with asymmetric outflow the branches flow-rate ratios were 0.65 (Left side on Fig. 1) and 035 of the inlet flow respectively.

The inlet velocity profile is assumed parabolic, given a mean flow velocity of 41.3 cm/s, a typical basilar artery diameter of 0.475 cm, and the kinematic viscosity of blood at 0.035 cm^2/s, the mean Reynolds number is 560. It should be noted that the numerical simulations were performed here for the fluid used in the experimental work of Cole (2004), with fluid kinematic viscosity at 0.14 cm^2/s, in addition the model has twice the diameter of a basilar artery, and therefore the input velocity needed to be doubled compared to physiological conditions to 82.53 cm/s. The application of pulsatile inflow also makes it necessary to match the Womersley number α with physiological conditions. It should be noted that with the model diameter twice physiological and the working fluid four times as viscous as blood, it is unnecessary to change the pulse frequency, this frequency is taken nominally here as 1 Hz.

The waveform shape was taken from an average waveform measured at the common carotid artery found in the literature, Berger and Jou (2000), and used by Cole (2004), Figure 2 shows the pulse with the fluid acceleration and deceleration phases during the systole and dias-
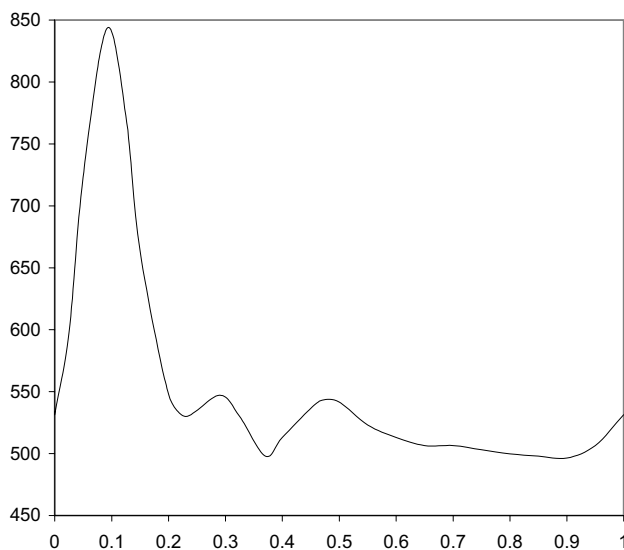
Figure 2 : Physiological waveform, mean Reynolds number Re=560.

tole respectively. The maximum and minimum Reynolds number are Re_{max}=842 and Re_{min}=498.

3   Numerical Method

The governing equations (1) and (2) were solved with the software Fluent v6.0 (Fluent, Inc., Lebanon, NH), which uses finite volume method for the spatial discretization. The interpolations for velocities and pressure use power law and second order respectively. The pressure-velocity coupling is obtained using the SIMPLEC algorithm. A explicit time-marching scheme with a small time step Δt=5x10^{-5} s was used for the computed grid size. Very fine unstructured grids with 197807 and 202515 cells were used for the model 1 and 2 respectively, the unstructured grids were composed primarily of tetrahedral mesh elements but included hexahedral, pyramidal, and wedge elements where appropriate.

To check grid independence, numerical simulations of the flow in the model 2 with symmetric outflow were performed on grids with 20% more and less elements respectively. Differences on local skin coefficients on several points of the aneurysm between the grids were small.

The workstation used to perform the simulations in this work had a Pentium IV processor of 2.8 Ghz clock speed, 1.5 Gb RAM memory, and running on Linux Redhat v.8.0 operating system. The run time for one case based on 4 consecutive pulsatile flow cycles that uses 8x10^4 iterations was approximately 190 hours of real time.

4   Results and Discussion

Figure 3 shows intra aneurismal flow in the middle planes X-Y and Y-Z, see Fig. 1, for the model 1 with symmetric, Fig. 3 (a) and (b), and asymmetric outflow conditions, Fig. 3 (c) and (d), with Re=560. The instantaneous velocity fields are shown for computational times of 3.1s and 3.7s, these times are representative of the systole and diastole respectively, see Fig. 2. The intra aneurismal flow shows a complex vortex structure. The asymmetry of the outflow affects the intra aneurismal flow, and the structure of the vortices. The intra aneurismal velocities are lower in the diastole phase, due the strong deceleration of the inflow.

Figure 4 shows intra aneurismal flow in the middle planes X-Y and Y-Z, with physiological representative waveform of inflow for the model 2 for symmetric and asymmetric outflow conditions, Fig. 4 (a), (b), and Fig. 4 (c), (d) respectively. The instantaneous velocity fields are shown for the computational time of 3.1s, this time corresponds to the maximal inflow velocity or the end of the accelerating phase of systole, and 3.7s or diastole. The asymmetry of the outflow affects the intra aneurysmal flow, and the flow near the aneurysm tip has a bigger stagnant region compared with the recirculation in model 1 in the cases with asymmetric outflow.

The inflow and outflow zones in the aneurysm neck in both models can be observed from Fig. 3 and 4. The aneurysm neck did not demonstrated a simple flow pattern, as was previously supposed in ideally shaped experimental aneurysms in vitro and in vivo. The long-term anatomical durability of coil embolization of aneurysms by using existing microcoil technology depends of the aneurysm form as the blood flow dynamics in the aneurysm neck, ideally the coil must be inserted in the inflow zone, to avoid flow recanalization. The flow dynamic after the aneurysm in the branches has secondary motion resulting from the turning of the stream as it enters these vessels, flow separation was observed in both models at the interior side of the "T" as result from the sharp turn the flow makes as it enters the junction.

Experimental flow visualization for models 1 and 2 in the middle plane X-Y are shown in Fig. 5. The cases have physiological representative waveform of inflow
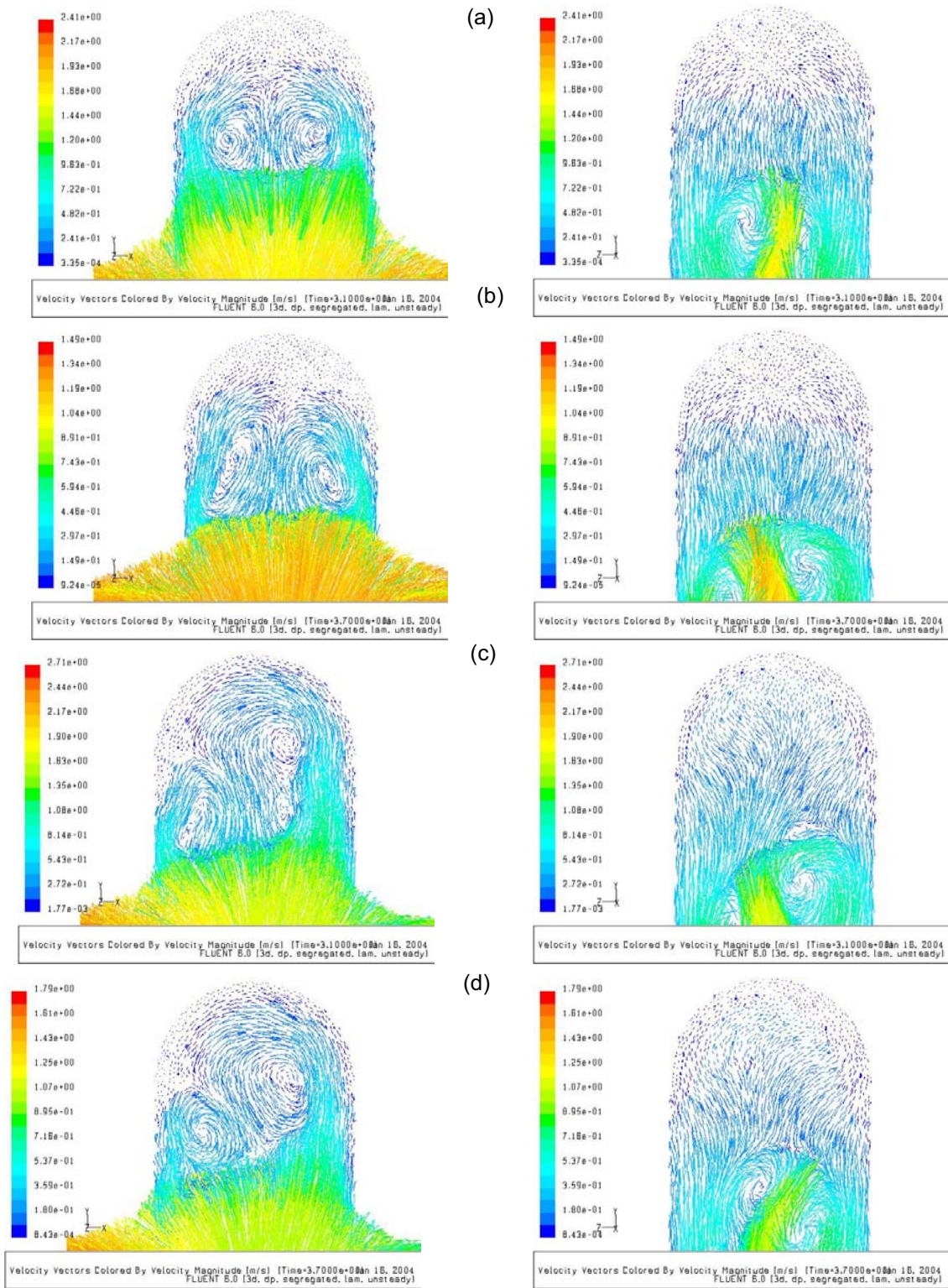
Figure 3 : Velocity vectors for model 1 at planes X-Y with Z=0, and Y-Z with X=0. (a) systole at 3.1s with symmetric outflow, (b) diastole at 3.7s with symmetric outflow, (c) systole at 3.1s with asymmetric outflow, (d) diastole at 3.7s with asymmetric outflow.
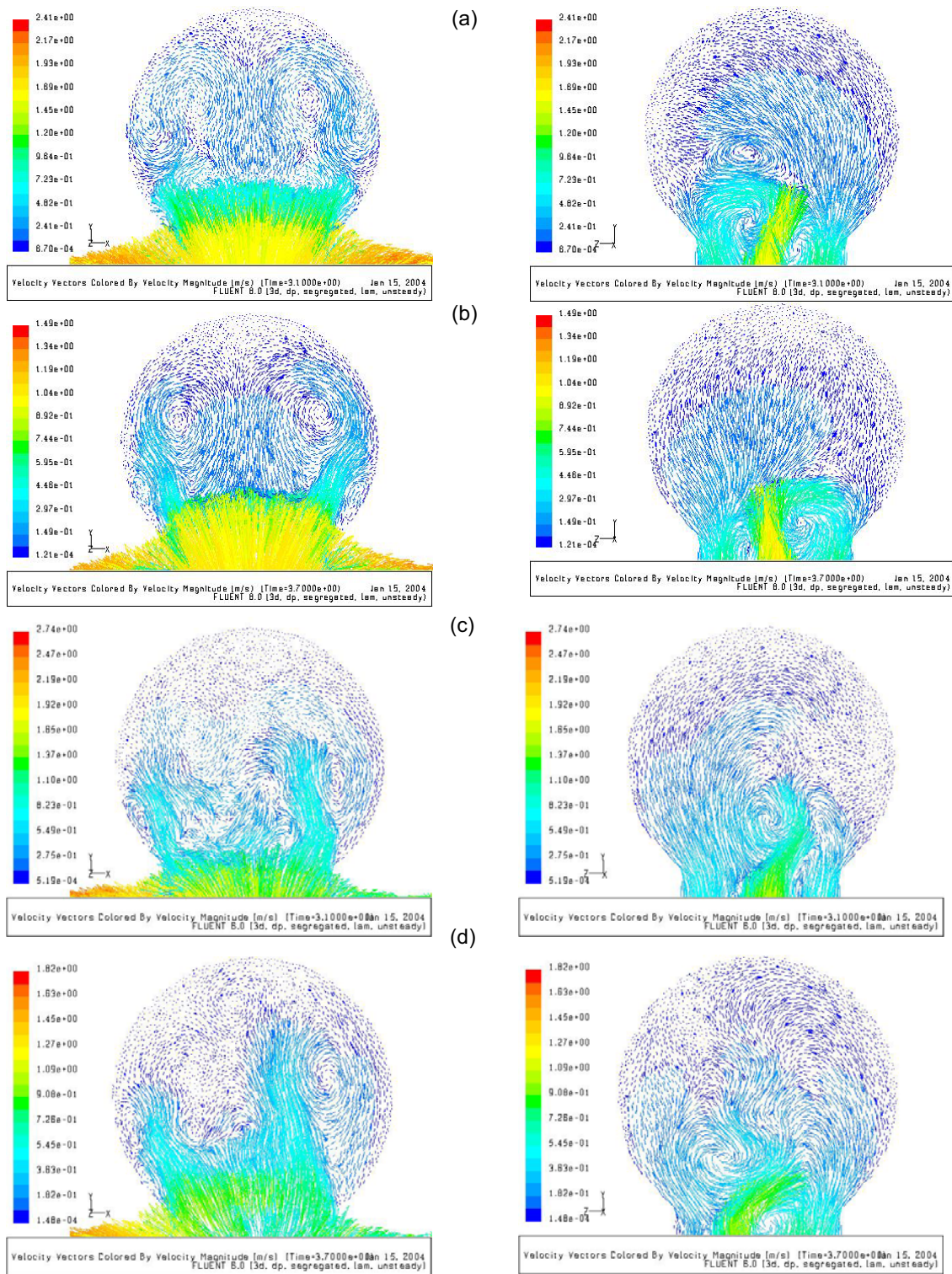
Figure 4 : Velocity vectors for model 2 at planes X-Y with Z=0, and Y-Z with X=0. (a) systole at 3.1s with symmetric outflow, (b) diastole at 3.7s with symmetric outflow, (c) systole at 3.1s with asymmetric outflow, (d) diastole at 3.7s with asymmetric outflow.
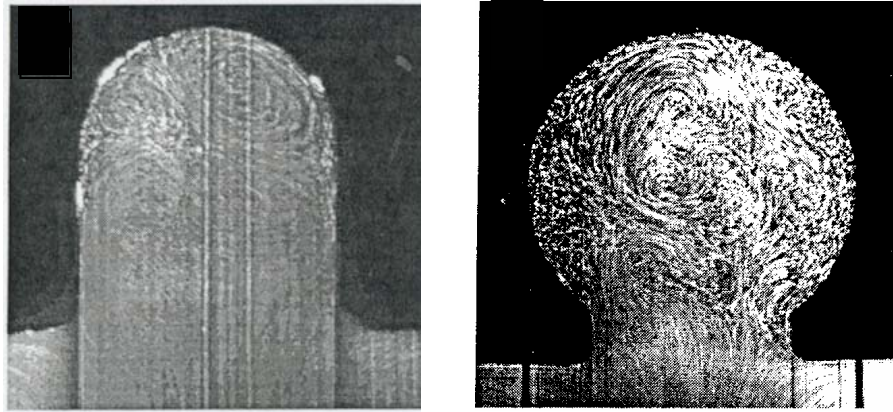
Figure 5 : Experimental flow visualization in models 1 and 2 on plane X-Y with Z=0 at peak systole. Cases with physiological waveform of inflow and asymmetric outflow, Re=560, Cole et al. (2004).
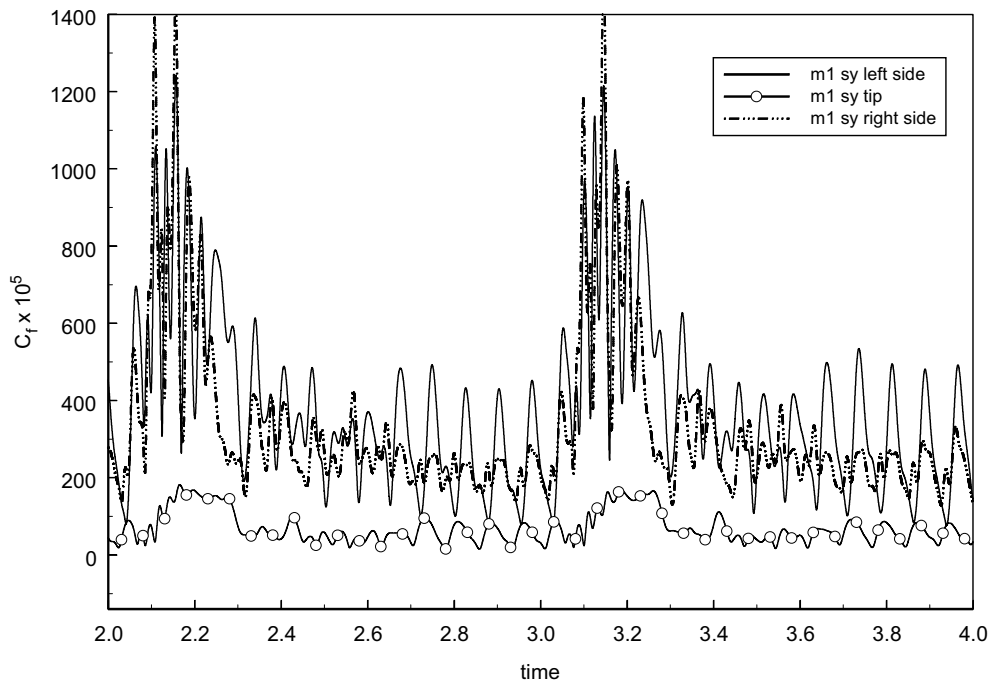
Figure 6 : Skin friction coefficient on three points of the aneurysmal wall plotted over two time cycles for the case with symmetric outflow in model 1.

and asymmetric outflow with Re=560, Cole et al. (2004). At peak systole, the flow in the tip of aneurysm for model 1 displays a significant quantity of unsteadiness and multiple vortices. In model 2 the unsteadiness of flow reaches the aneurysm tip, there is a large vortex generation beyond the neck. The comparison with the calculated velocity fields, Fig. 3 (c) and Fig. 4 (c), shows differences on vortex structure, one explication can be that the experimental flow undergoes on a early transition to turbulence.

Time dependence over two times cycles of skin friction coefficient on three points on the aneurysm wall in the middle plane X-Y, see Fig. 1, for model 1 with symmetric and asymmetric outflow show Fig. 6 and 7 respectively. The asymmetry of the outflow increases the wall shear stress on the aneurysm wall. It is remarkable with both
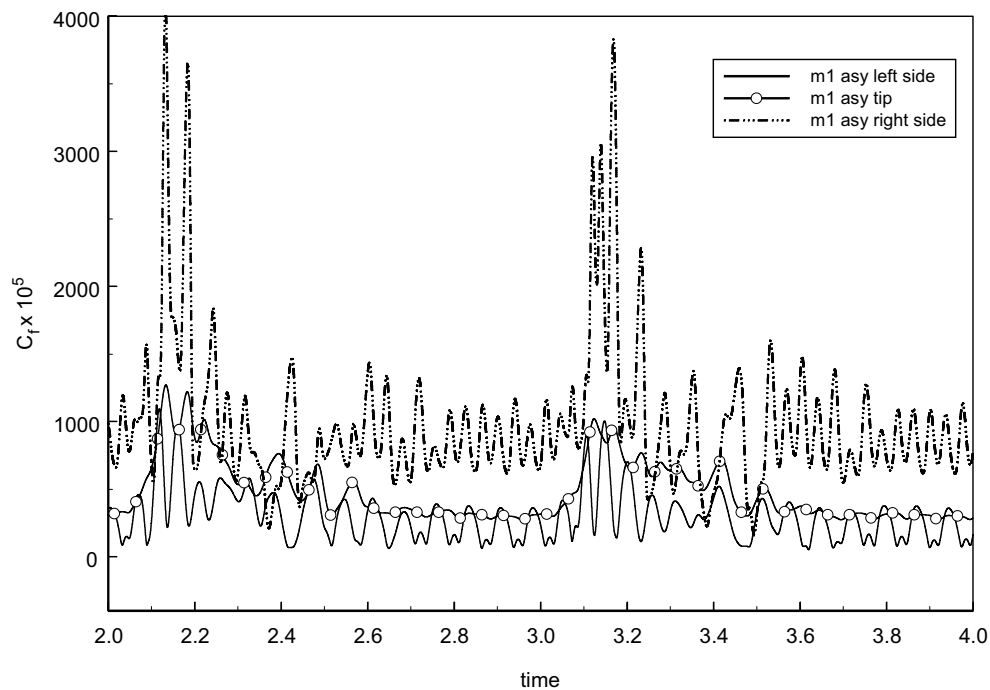
Figure 7 : Skin friction coefficient on three points of the aneurysmal wall plotted over two time cycles for the case with asymmetric outflow in model 1.

outflow conditions the time modulation of skin friction coefficient with the waveform of inlet velocity.

Figures 8 and 9 show time dependence of skin friction coefficient on model 2 in three different points of plane X-Y for Z=0, see Fig. 1, on the aneurysm surface for the cases with symmetric and asymmetric outflow respectively. The modulation of skin friction coefficients with the waveform of inflow is not so strong as in model 1. The values of skin friction coefficient do not increase with asymmetric outflow. The values on point L and R are similar with asymmetric outflow, due the low fluid velocities in these regions of the aneurysm.

Cole et al. (2004)reported that the maximum shear stress that occur at the aneurysm tip with pulsatile input and asymmetric outflow on model 1 approaches 10Pa on the model. The numerical calculated maximum value of wall shear stress from Fig. 7 for this case reaches 11Pa at the pick systole. The numerical prediction of wall shear stress matches well with the experimental, in spite the differences among numerical and experimental determined velocity fields and the additional difficulty to measure wall shear stress from velocity fields of very low magnitude.

Damage to the endothelium is seen as a contributing cause to aneurysm growth and rupture. Once the integrity of this layer of cells lining the lumen is breached, subsequent damage to the structural fibers of the vessel may occur. Fluid mechanics is involve in the process leading to the damage of the endothelium. The correlation between fluctuating shear stresses and endothelial degeneration has been well documented in the literature. In this work were found local shear stresses that showed big variation with time and position on the aneurismal surface. This result suggests a damage mode involving high amplitude shear stresses. This damage mode could include elements of fatigue as consequence of the big variation of wall shear stresses, in addition the small velocities on the aneurysm can encourage thrombosis.

This numerical study of flow hemodynamics provides insight into the vortex dynamics and wall shear stresses originated in hypothetical geometries of saccular aneurysms in the basilar artery. However further investigations are required to consider the interaction of the compliant wall of the aneurysm, transition to turbulence, and anatomically realistic geometry.
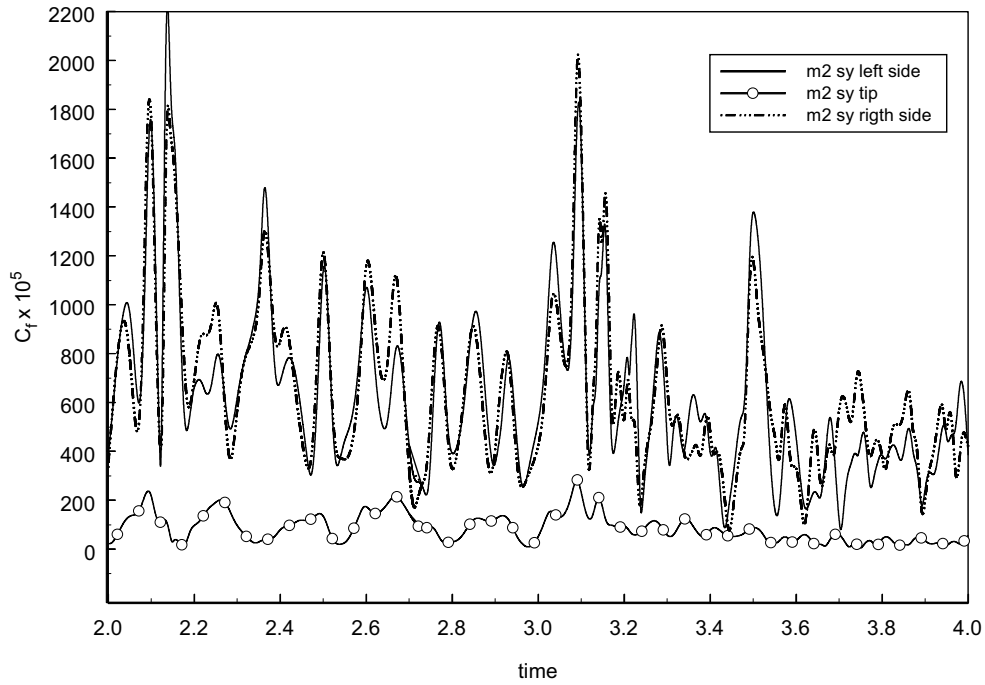
Figure 8 : Skin friction coefficient on three points of the aneurysmal wall plotted over two time cycles for the case with symmetric outflow in model 2.
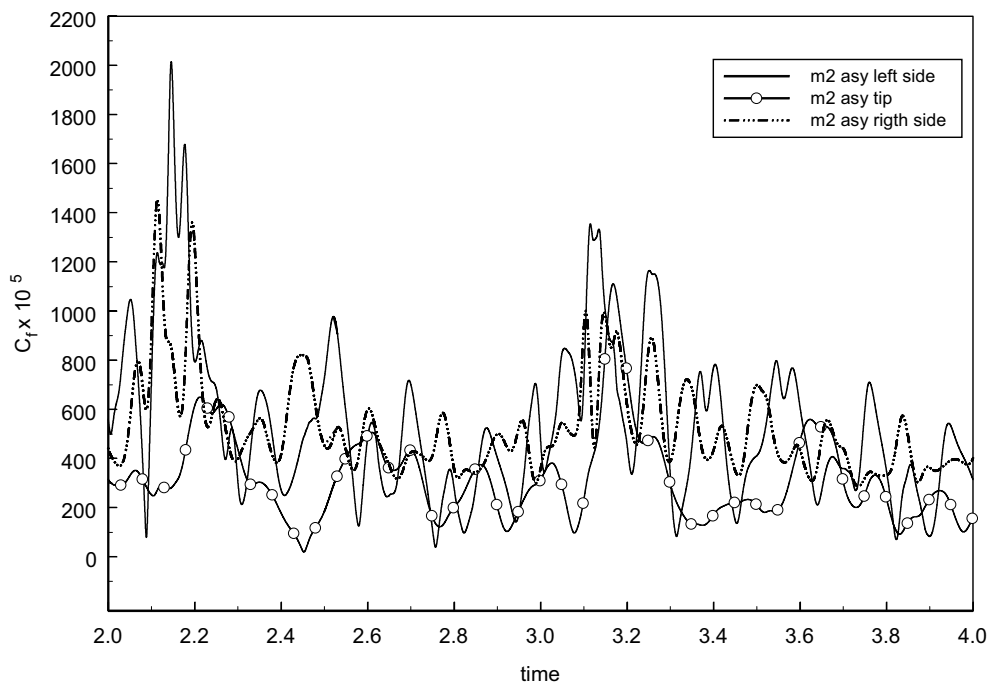
Figure 9 : Skin friction coefficient on three points of the aneurysmal wall plotted over two time cycles for the case with asymmetric outflow in model 2.

5   Conclusions

The present work study unsteady fluid flow and wall shear stress in two models of terminal saccular aneurysm of the basilar artery. Each model is subject to physiological representative waveform of inflow for a mean Reynolds number of 560. The effects of aneurysm form and asymmetric outflow rates are studied in detail. The flow shows a unsteady complex vortex structure, and the flow in the aneurismal neck has defined inflow and outflow zones. The wall shear stresses in the aneurysm show big temporal and spatial variations. The aneurysm wall is subject to a shear stress with high amplitude that oscillates with the frequency of the inflow.

Nomenclature

C_f	skin friction coefficient = $\tau_W/(1/2\rho U_o^2)$
Re	Reynolds number = $U_o d/\nu$
U_o	mean velocity at inlet
d	diameter
p	pressure
u	velocity

Greek symbols

α	Womersley number = $(\omega\, d^2/\nu\,)^{0.5}$
μ	fluid viscosity
ν	fluid kinematic viscosity = μ/ρ
ρ	density
ω	cardiac frequency

References

Berger, S. A.; Jou, L. D. (2000): Flows in stenotic vessels, *Annu. Rev. Fluid Mech.*, 32 347-382.

Cole, R. H.; Selby, K.; Saloner, D.; Savaş, Ö. (2004): Flow visualization and digital particle image velocimetry on model bifurcation aneurysms, To appear in *Journal of Biomechanical Engineering*.

Ernemann, U.; Grönewäller, E.; Duffner, F. B.; Guervit, O.; Claassen, J.; Skalej, M. D. (2003): Influence of geometric and hemodynamic parameters on aneurysm visualization during three-dimensional rotational angiography: an in vitro study, *AJNR Am J. Neuroradiology*, 24 597-603.

Foutrakis, G.; Yonas, H.; Sclabassi, R. (1999): Saccular Aneurysm formation in curved and bifurcating arteries, *AJNR Am. J. Neuroradiology*, 20 1309-1317.

Gijsen, F. J.; van de Vosse, F. N.; Janssen, J. D. (1999): The influence of the non-Newtonian properties of blood on the flow in large arteries: steady flow in a carotid bifurcation model, *J. of Biomechanics*, 32 601-608.

Hoh, B. L.; Putman, C. M.; Budzik, R. F.; Carter, B. S.; Ogilvy, C. S. (2001): Combined surgical and endovascular techniques of flow alteration to treat fusiform and complex wide-necked intracranial aneurysms that are unsuitable for clipping or coil embolization, *J. Neurosurgery*, 95 24-35.

Ku, D. N. (1997): Blood flow in arteries, *Annu. Rev. Fluid Mech*, 29 399-434.

Liou, T. M.; Liou, S. N. (1999): A Review on in vitro studies of hemodynamic characteristics in terminal and lateral aneurysm models, *Proc. Natl. Sci. Counc. ROC(B)*, 23 133-148.

Parlea, L.; Fahrig, R.; Holdsworth, D. W.; Lownie, S. P. (1999): An analysis of the geometry of saccular intracranial aneurysms, *AJNR Am. J. Neuroradiol*, 20 1079-1089.

Schievink, W. I. (1997): Intracranial Aneurysms, *The New England Journal of Medicine*, 336 28-40.

Steinman, D. A.; Milner, J. S.; Norley, C. J.; Lownie, S. P.; Holdsworth, D. W. (2003): Image-based computational simulation of flow dynamics in a giant intracranial aneurysm, *Am. J. Neuroradiology*, 24 559-566.

Tateshima, S.; Murayama, Y.; Villablanca, J. P.; Morino, T.; Takahashi, H.; Yamauchi, T.; Tanishita, K.; Viñuela, F. (2001): Intraaneurysmal flow dynamics study featuring an acrylic aneurysm model manufactured using a computerized tomography angiogram as a mold, *J. Neurosurgery*, 95 1020-1027.

Tateshima, S.; Viñuela, F.; Villablanca, J. P.; Murayama, Y.; Morino, T.; Nomura, K.; Tanishita, K. (2003): Three-dimensional blood flow analysis in a wide-necked internal carotid artery-ophthalmic artery

aneurysm, *J. Neurosurgery*, 99 526-533.

Ujiie, H.; Tachibana, H.; Hiramatsu, O.; Hazel, A. L.; Matsumoto, T.; Ogasawara, Y.; Nakajima, H.; Hori, T.; Takakura, K.; Kajiya, F. (1999): Effects of size and shape (aspect ratio) on the hemodynamics of saccular aneurysms: a possible index for surgical treatment of intracranial aneurysms, *Neurosurgery*, 45 119-130.

Weir, B.; Amidei, C.; Kongable, G.; Findlay, J. M.; Kassell, N. F.; Kelly, J.; Dai, L.; Karrison, T. G. (2003): The aspect ratio (dome/neck) of ruptured and unruptured aneurysms, *J. Neurosurgery*, 99 447-451.

Zhao, S. Z.; Xu, X. Y.; Hughes, A. D.; Thom, S. A.; Stanton, A. V.; Ariff, B.; Long, Q. (2000): Blood flow and vessel mechanics in a physiologically realistic model of a human carotid arterial bifurcation, *J. of Biomechanics*, 33 975-984.